SUPPORTING INFORMATION

The importance of substrate pore size and wetting behavior in gas diffusion electrodes for CO_2 reduction

Alessandro Senocrate, Francesco Bernasconi, Daniel Rentsch, Kevin Kraft, Matthias Trottmann, Adrian Wichser, Davide Bleiner, and Corsin Battaglia*

Empa, Swiss Federal Laboratories for Materials Science and Technology, Überlandstrasse 129, 8600 Dübendorf (CH)

**alessandro.senocrate@empa.ch*

1. Experimental methods

1.1. GDE fabrication

GDEs are obtained by sputtering a metal layer (typically Ag) on one side of a commercial hydrophobic polymer substrates made either of PVDF (Durapore, Merck) or of PTFE (Advantec or Sterlitech). The hydrophobic fiber substrates are used as obtained. Relevant microstructural features are given in Table S1. As these substrates are typically used for filtering purposes, their nominal pore size reflects more their filtering ability, and does not accurately represent their mean pore size. For this reason, we carried out porosimetry experiments (described below) to extract their mean pore size (also given in Table S1). The sputtering process is carried out in DC mode, with a typical power of 100 W, an Ar pressure of 0.004 mbar, and a deposition rate of 0.7 nm/sec for Ag, measured by quartz microbalance. Deposition times are adjusted to yield a metal layer of approximately 500 nm thickness. Sheet resistance of the obtained GDE is found below 0.5 Ω/cm, irrespective of the substrate pore size. This is negligible compared to the final cell resistance, as our typical testing cell has a large distance (> 1 cm) between anode and cathode, leading to cell resistances in the order of 10 Ω in the 1 M $KHCO_3$ electrolyte used.

Polymer	Brand	Nominal pore size (µm)	Mean pore size (µm)	Thickness (µm)
PTFE hydrophilic	Advantec	0.1	0.3	35
PTFE	Sterlitech	0.2	0.3	25-50
PTFE	Sterlitech	0.45	0.4	25-50
PTFE	Sterlitech	1.0	2.8	200-300
PVDF	Durapore	0.1	0.3	125
PVDF	Durapore	0.2	0.4	125
PVDF	Durapore	0.45	0.8	125

Table S1. Commercial polymer substrates used in this work. Nominal pore sizes and thickness are taken from the manufacturer.

1.2. SEM imaging

Secondary Electron Microscopy imaging was performed using a tabletop SEM (Hitachi TM3000) with 15 kV electron acceleration voltage. Due to severe charging effects caused by the highly resistive nature of the hydrophobic polymers used, the samples were analyzed and compared after the Ag metal deposition. The FIB cross-sections were prepared by a Helios 5 UX (Thermo Scientific). A protective carbon layer was first deposited on the ROI at 30 kV (90 pA), then milled at 30 kV (1.2 nA) and finished at 30 kV (41 pA). SEM images were recorded on the same instrument at 2 kV (0.1 nA).

1.3. Electrochemical analysis

To test the selectivity and activity of the prepared GDE, these were inserted in a modified PEEK electrochemical cell (Redox.me) with a round active area of 1 cm^2. The electrolyzer, shown in Fig. S1, consists of 3 chambers, one dedicated to the CO_2 gas flow (3 mL), and two for the cathodic and anodic electrolytes (catholyte and anolyte, 15 mL each). The GDEs are used as cathodes, with their hydrophobic polymer side facing the CO_2 gas, and the active side hosting the sputtered metal catalyst facing the catholyte. A Nafion 117 membrane is used in all experiments to separate the two liquid chambers, to avoid product crossover. The catholyte chamber hosts the reference electrode (Ag/AgCl in saturated KCl) and the anolyte chamber the anode (IrO_x electrodeposited on a Ti gauze). The CO_2 gas flow is controlled by Mass Flow Controllers (Bronkhorst) and set in the range of 30 mL/min. The main gaseous products, e.g. CO,

leave the electrolyzer preferentially from the gas compartment. The gas flow leaving the GDE and containing products is also flushed through the catholyte chamber to collect any products formed on that side, before being injected in a gas chromatography for analysis.

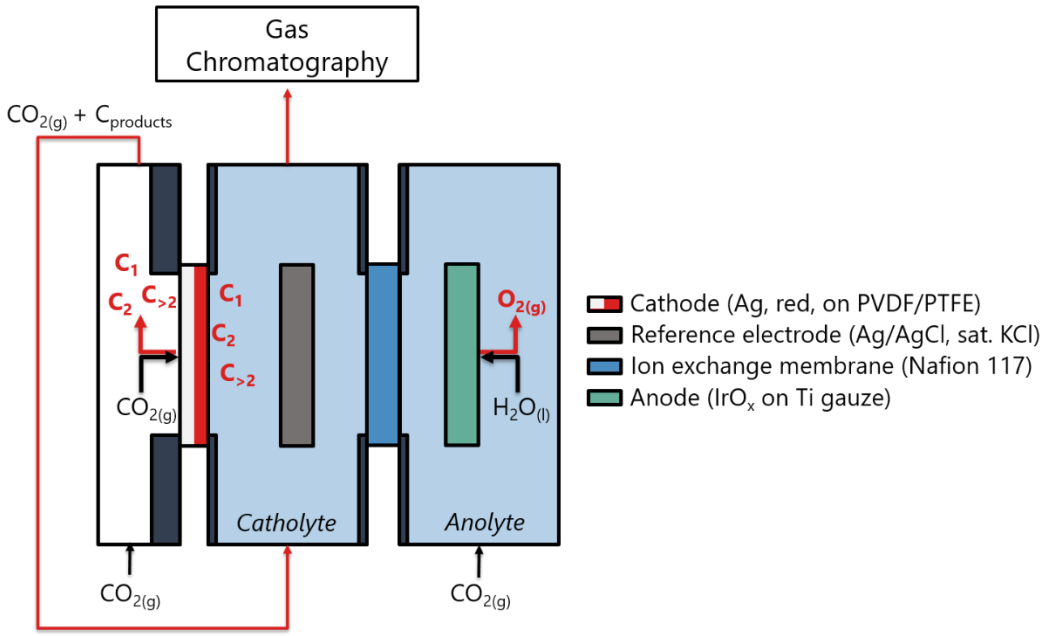

Figure S1. Schematics of the electrolyzer cell used for the electrochemical characterizations.

The electrolyte used in all characterization was 1 M $KHCO_3$ (99.7 % ACS, Alfa Aesar). Conductive Al tape is used as an electrical contact, but no area of the tape is exposed to the liquid electrolyte nor to the CO_2 gas. In a typical experiment, the GDE is loaded and the CO_2 flow is started. The 1 M $KHCO_3$ electrolyte is saturated with CO_2 by bubbling the gas in both chambers in two separate streams. The electrolysis is started after saturation, with an initial linear scan voltammetry to reach the desired conditions, and a subsequent chronoamperometric step to apply the desired current for the duration of 1 h. Before the start of the 1h electrolysis, and at the end, an impedance spectroscopy measurement is performed to assess the cell resistance and its variations. The voltage of the working electrode (E_{WE}) is corrected for this resistance, and normally both the E_{WE} starting value and the E_{WE} end value (after 1 h) are corrected for their respective impedance measurements, to verify that there were no significant variations in the electrochemical conditions experienced by the sample. In addition, the E_{WE} value is corrected for the reference electrode shift to be brought back in the RHE scale. The reference electrode shift is measured with respect to a pseudo reversible hydrogen electrode, obtained by trapping a bubble of H_2 in contact with a Pt wire, which is immersed in 1 M H_2SO_4. Typical shift values for our Ag/AgCl reference electrodes (saturated KCl) are within 5 mV of the thermodynamic value (199 mV). Electrochemical surface areas are assessed by means of electrical double layer capacitance. In a typical experiment, a cyclic voltammetry is performed on a GDE before starting the electrolysis (i.e., in 1 M $KHCO_3$), and after 1 h of CO_2 reduction. The voltammetry scans the range from -0.1 to +0.1 V in RHE, with a variable scan rate between 100 and

500 mV/sec. An Ag foil (Alfa Aesar) used as a reference in the same electrolyte yields a specific capacitance of 49.3 ± 1.1 uF/cm^2.

1.4. Product analysis

During the 1h electrolysis, the gas leaving the electrolyzer is bubbled through the catholyte chamber (to collect the CO_2RR products released in the liquid) and subsequently connected to a gas chromatographer (MicroGC Fusion, Inficon), with a Molecular Sieve (Ar as carrier gas) and a RT-Q (He as carrier gas) columns. The GC samples the gas flow every 5 minutes, to yield a time resolved product analysis. The gas flow is also measured at the entrance of the GC using a Volumetric Mass Flow Meter (Defender, MesaLabs).

The Faradaic Efficiency for the gases is calculated using the following formula:

$$FE_{gas,x} = \frac{\mathrm{W}\left(\mathrm{STP}, \frac{\mathrm{L}}{\mathrm{min}}\right) \cdot \mathrm{t\ (min)} \cdot [c]_{gas,x} \cdot n_{e,x} \cdot F\ (\frac{C}{mol})}{\mathrm{Q\ (C)} \cdot 22.414\ (\frac{\mathrm{L}}{\mathrm{mol}})} \cdot 100$$

where W is the gas flow measured by the flow meter at standard temperature and pressure, t is the electrolysis time, $[c]_{gas,x}$ is the concentration of the gaseous product x (fraction of the gas flow taken up by the product x, adimensional), $n_{e,x}$ is the electrons required to produce product x, F is the Faraday constant, and Q is the charge passed during the electrolysis time, measured by the potentiostat.

The liquid product analysis was normally performed using ^{1}H nuclear magnetic resonance spectra (NMR, Avance III 400 NMR spectrometer, Bruker) recorded at 400.1 MHz and at 298 K, using the procedure given in Ref. [1,2]. Briefly, NMR samples are composed of 1500 µL of the electrolyte containing the liquid products, then 150 µL of a 10 mM dimethyl sulfoxide (DMSO, 99.8+ %, Alfa aesar) as an internal standard solution and 100 µL of D_2O were added and the solution thoroughly mixed before analysis. The ^{1}H NMR spectra were recorded with lock on D_2O using the gradient selected composite pulse sequence "zgcpgppr" with a 4 s long presaturation of the water resonance at 4.7 ppm to eliminate the water signal. A long recycle delay of 60s was applied since formic acid HCOOH (the only product detected in the liquid phase) shows a long T_1 relaxation time in the order of 20 s.[3] For the long-term experiments, liquid products were instead analyzed using high performance liquid chromatography (Agilent 1260), with a refractive index detector, a HiPlex H column and a flow of 0.6 mL/min of 5 mM H_2SO_4 as an eluent.

The Faradaic Efficiency for the liquid products is calculated with the following equation:

$$FE_{liquid,y} = \frac{\mathrm{V\ (L)} \cdot \mathrm{t\ (min)} \cdot [c]_{liquid,y}\left(\frac{\mathrm{mol}}{\mathrm{L}}\right) \cdot n_{e,y} \cdot F\left(\frac{C}{mol}\right)}{Q\ (C)} \cdot 100$$

where V is the electrolyte volume, t is the electrolysis time, $[c]_{liquid,y}$ is the molar concentration of the liquid product y, $n_{e,y}$ is the number of electrons required to produce liquid product y, F is the Faraday constant, and Q is the charge passed during the electrolysis time. For accuracy, the electrolyte volume was inserted in the electrolysis cell using a 10 mL adjustable volume pipette (Eppendorf).

1.5. Porosimetry and water entry pressure measurements

Pore size and water entry pressure (WEP) measurements are carried out using a Porosimetry system (Porolux 1000, Porometer) with liquid permeability capability. For the mean pore size measurement, the substrate under examination (13 mm diameter) is first soaked in a fluorinated hydrocarbon (PoreFill liquid, Porometer) and an increasing pressure of N_2 gas is imposed on top of the substrate, until first displacement of the liquid takes place (bubble point). The pressure is further increased and the permeability at various pressures is measured, in a procedure called a "wet" curve. Subsequently, a "dry" curve, i.e. the same measurement without soaking the substrate in the liquid, is performed. An example of the two curves is given in Fig. S2. From the two curves, the mean pore size and pore size distribution can be obtained using the Young Laplace equation and the following formula:

$$W = \frac{-\rho\pi R_b^2 k_b \Delta P}{\eta L_b}$$

Where W is the fluid mass flow, R_b is the sample width, L_b is the sample length, ρ is the fluid density, η is the fluid viscosity, k_b the sample permeability, and P is the pressure applied.

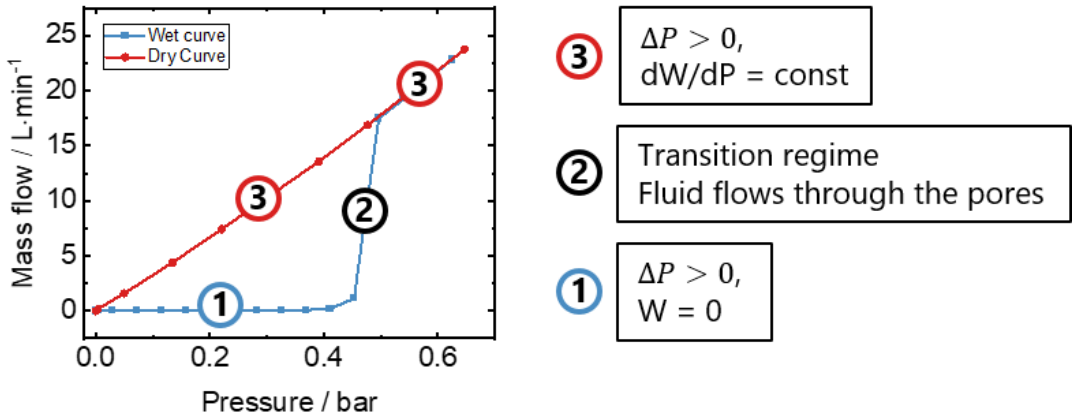

Figure S2. Typical wet and dry porosimetry curves recorded for the determination of the mean pore size of the porous substrate.

For the WEP measurement, a dry substrate (25 mm diameter) is used and deionized water is slowly pressurized on top of the substrate until it starts permeating. A laboratory scale is used to record the amount of water that passes through the porous substrate. The first consistent increase in weight, typically in the order of 100 mg, is used to determine the WEP.

1.6. Chemical analyses

Chemical analyses were carried out by X-Ray Fluorescence (XRF), and laser ablation inductively coupled plasma mass spectroscopy (LA-ICP-MS). XRF was carried out on ZSX PrimusIV from Rigaku. For LA-ICP-MS, the samples were measured using a custom-made setup, consisting of a Nd: YAG Laser (Qsmart by Quantel), sample stage and NExION 2000 ICP-MS (Perkin Elmer). The samples were fixed on a double-sided C adhesive tape and ablated using the 2nd harmonic of the laser (532 nm) with an intensity of 5 mJ and a spot size of 200 µm. The generated aerosols were fed into the ICP-MS directly by means of an Argon carrier gas through Tygon tubing, then ionized in the plasma and analyzed after mass resolution. The limit of detection for this method is in the sub-ppm range. For the LA-ICP-MS calibration, we used Ag ingots with known and certified amount of Cu impurities (Breitlander GmbH). Cu amounts in the standards were 0.00184 at. %, 0.0108 at. % , and 0.049 at. % vs Ag.

2. Porosimetry measurements before/after metal deposition

To check for possible variation of the microstructural properties by metal deposition, we performed porosimetry experiments before and after coating the metal layer onto the hydrophobic substrates. As shown in Fig. S3, no substantial changes in the pore size distribution were observed.

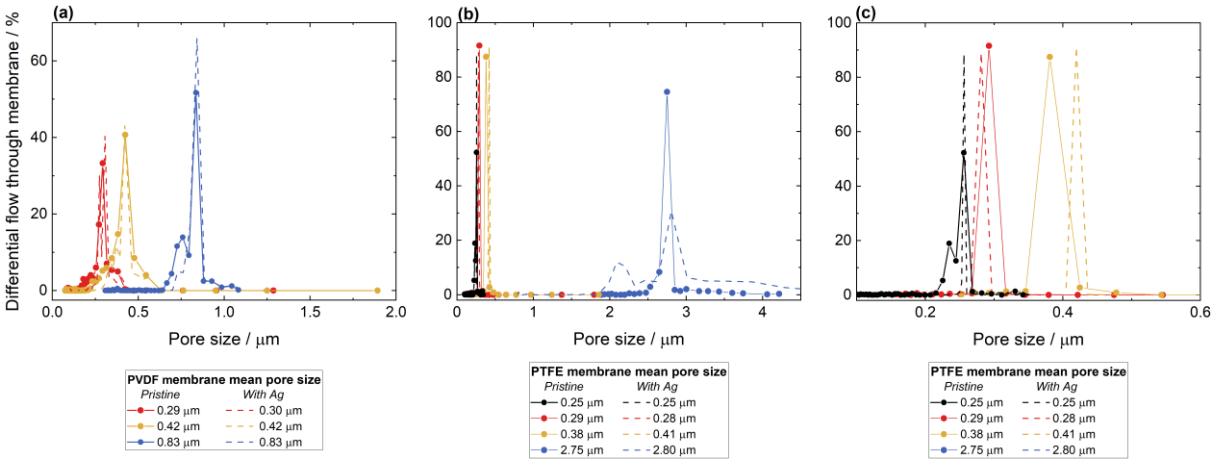

Figure S3. Complete porosimetry measurements and mean pore size for the set of **(a)** PVDF and **(b)** PTFE substrates used in this study. **(c)** shows a zoomed version of panel (b) for additional clarity. Negligible differences are present between before and after metal deposition.

3. X-ray diffraction

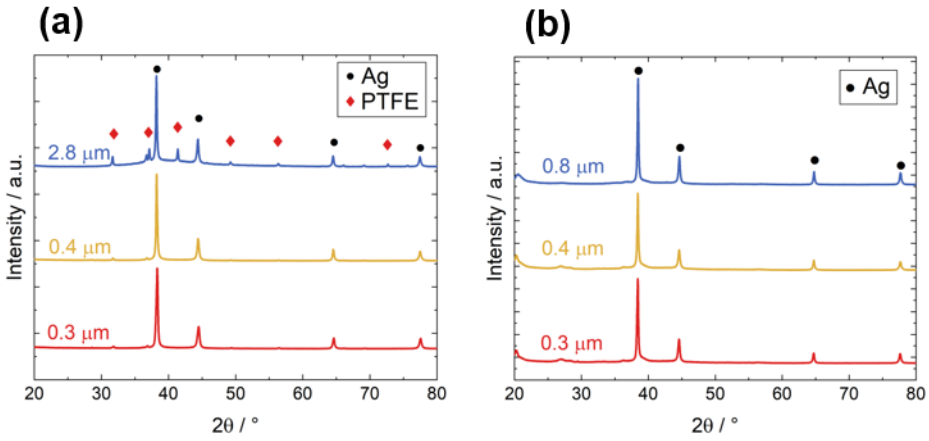

Figure S4. XRD measurements after Ag deposition for the set of **(a)** PTFE and **(b)** PVDF substrates used in this study. Only the reflections for Ag are visible on the PVDF substrates, while PTFE substrates show also diffraction peaks due to the polymer.

4. SEM images of all substrates

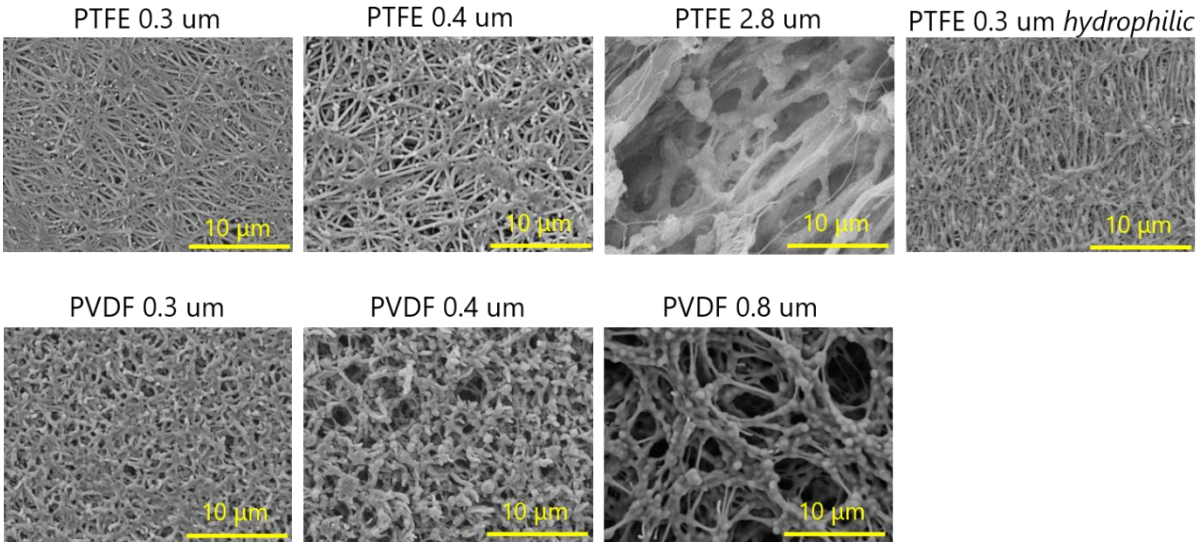

Figure S5. SEM images of commercial polymer substrates studied in this work, all coated with a 500 nm Ag layer.

5. Electrochemically active surface area measurements

To rule out possible differences in the electrochemically active surface area (ECSA) of the various GDEs, which could potentially cause differences in their selectivity, we carry out electrochemical double layer capacitance (EDLC) measurements. An Ag foil (Alfa Aesar) used as a reference yields a specific capacitance of 49.3 ± 1.1 uF/cm^2. ECSA was measured before and after performing the CO_2RR. Table S2 summarizes the results obtained from these experiments for all the GDEs. For all GDEs, ECSA is initially very similar, and increases as a function of electrolysis time. In general, no significant differences are visible

between the ECSA values of the different GDEs, with the possible exception of the one based on hydrophilic PTFE, which shows a relatively lower ECSA. Nonetheless, GDEs of drastically different selectivity and stability such as those based on PTFE substrates of 2.8 µm and 0.4 µm pore size showing almost identical surface areas, ruling out differences in ECSA as responsible for the difference in performance. Considering the changes in ECSA with CO_2 electrolysis time, it is tempting to connect these variations to an enhanced wetting of the GDEs by the electrolyte. However, due to the non-conductive nature of the hydrophobic polymer fibers used as substrates, we must note that an increased wetting or a flooding process would not be directly captured by the ECSA measurement. We cannot definitely rule out that some areas of metallized substrate would only get in contact with the electrolyte as a later stage of the electrolysis, yielding a higher surface area. However, to be detected by the ECSA measurement these areas must be electrically connected to the rest of the GDE, and somehow initially be prevented contact with the electrolyte, for example due to physical contact with a hydrophobic polymer fiber. While this occurrence is possible in our GDEs, we note that a more straightforward explanation for the ECSA enhancement is a minor surface reconstruction of the metal during the electrolysis.

GDE	**ECSA before CO_2RR (cm^2)**	**ECSA after 1 h CO_2RR (cm^2)**	**ECSA after 2 h CO_2RR (cm^2)**
	Before CO2RR	**1h**	**2h**
PTFE hydrophilic 0.3 µm	4.0	4.9	/
PTFE 0.3 µm	8.2	9.3	10.9
PTFE 0.4 µm	7.7	12.4	13.3
PTFE 2.8 µm	7.2	12.8	13.4
PVDF 0.3 µm	6.9	10.8	11.3
PVDF 0.4 µm	7.3	11.8	13.9
PVDF 0.8 µm	8.3	10.4	11.7

Table S2. ECSA values measured by means of EDLC for all GDEs in this study, before and after CO_2RR.

6. Product distribution including liquids as a function of pore size

The product distribution of all samples involved in the study of the pore size dependence was assessed including the liquid product formation. As seen in Fig. S5, only formic acid (HCOOH) could be detected in significant quantities, with considerable Faradaic efficiencies in the case of PVDF samples.

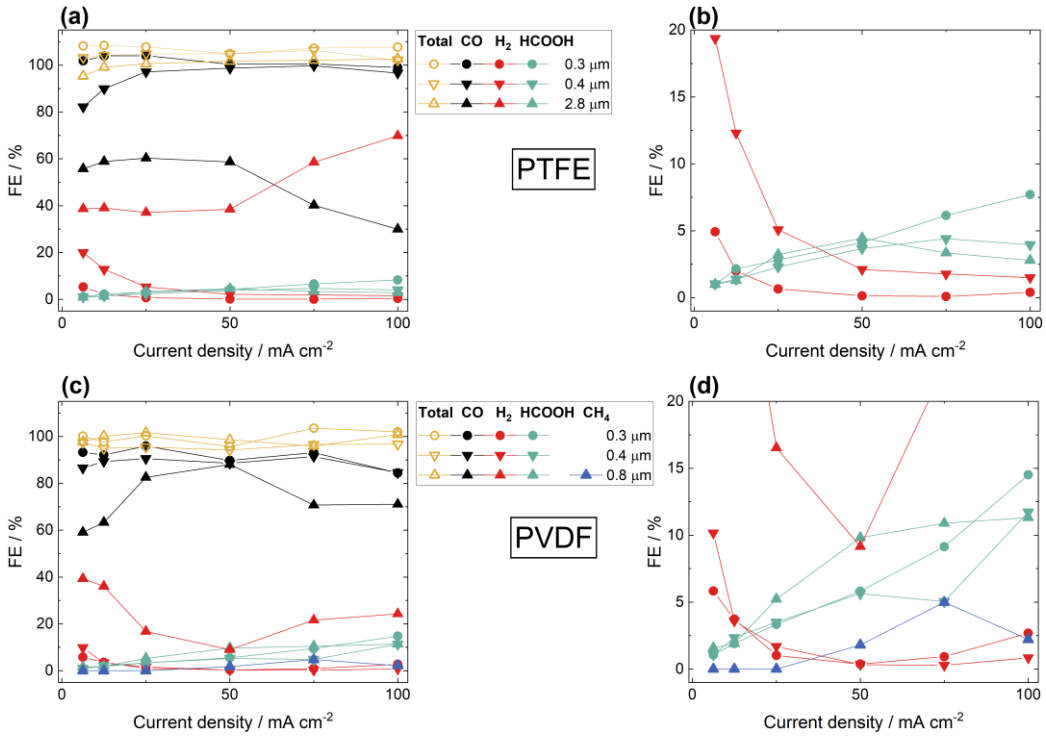

Figure S6. Product distribution (including liquid products) of all samples of **(a)** PTFE- and **(c)** PVDF-based GDEs shown in Fig. 2. For easier identification of the by-products, plots with a magnification of the range of FE< 20 % are shown in **(b)** and **(d)**.

7. Reproducibility of measurements

Due to the large volume of GDEs prepared and different experiments, we assessed the reproducibility of our characterization methods by repeating the CO_2 electrolysis experiment on 3 different PVDF-based GDEs of 0.8 um pore size (WEP of 1.6 bar). As shown in Fig. S13, by averaging FEs and cathode voltages over a 1-h electrolysis experiments at the highest current investigated of 100 mA/cm^2, we obtain reproducible results.

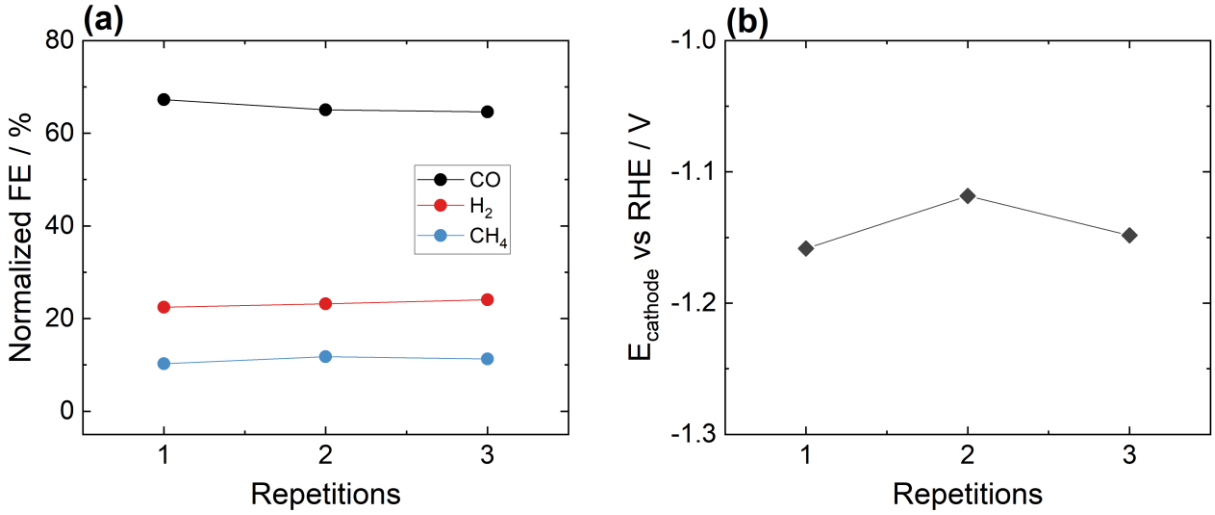

Figure S7. (a) Selectivity and **(b)** cathode voltage measurements for 3 different Ag coated PVDF-based GDEs, averaged over a 1 hour electrolysis experiment at 100 mA/cm^2.

8. Selectivity and activity vs GDE thickness

To test the effect of the thickness on the selectivity of the GDEs, we prepared hydrophobic porous substrates in-house by electrospinning a solution of PVDF-HFP (polyvinylydenfluoride-hexafluoropropylene) in dimethylformamide (DMF). Typical electrospinning parameters are: 20 kV voltage between the tip of the needle and a flat metal collector, 20 wt. % solution of PVDF-HFP in DMF with 1 wt. % TEABr salt, 8 cm tip-collector distance, 10 µL/min solution flow rate. In this way, we are able to reproduce pore sizes similar to the commercial substrates and accurately control their thickness. By varying the electrospinning time we obtain fiber mats in the range of 30-500 µm thickness, as measured with a micrometer. As shown in Fig. S7, for a substrate mean pore size of 0.3 µm, no significant difference is observed in the selectivity of samples ranging from 30 to 500 µm. We can therefore conclude that thickness does not plays an important role in this range. Note that all the commercial substrates studies fall within this range.

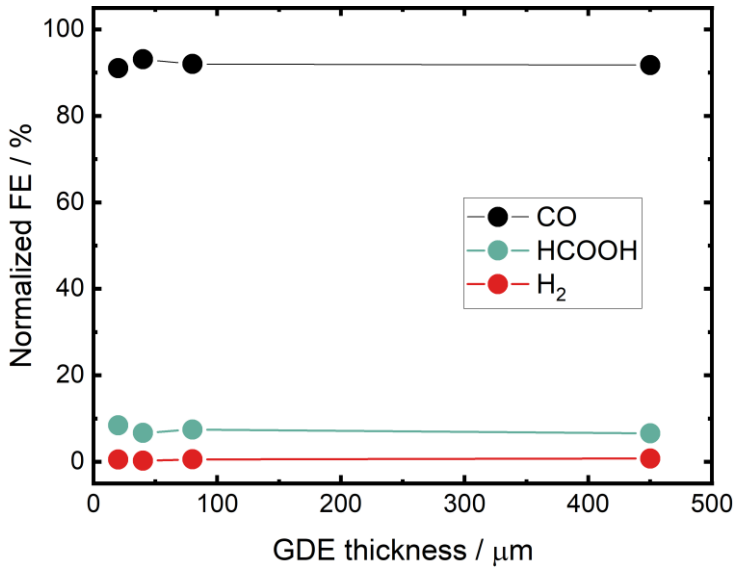

Figure S8. Faradaic efficiency as a function of thickness for a series of GDE made from electrospun PVDF-HFP substrates with identical pore size.

9. Water entry pressure measurements

As shown in Fig. S8, substrates with smaller pore sizes show a much higher WEP than substrates with large pores. For similar pore sizes, PTFE has a much larger WEP than PVDF due to its more intrinsic hydrophobic character, i.e. its higher water contact angle. We additionally verified that using 1 M $KHCO_3$, i.e. our CO_2RR electrolyte, as a fluid instead of water does not alter the WEP values. Indeed, a PTFE substrate of 0.4 µm pore size shows a WEP of 5.5 bar with $KHCO_3$, almost identical to the value of 5.7

bar obtained using H_2O. The same is observed for a PVDF substrate with 0.4 µm pore size, which yields a WEP of 2.7 bar with $KHCO_3$, and 2.6 bar with H_2O.

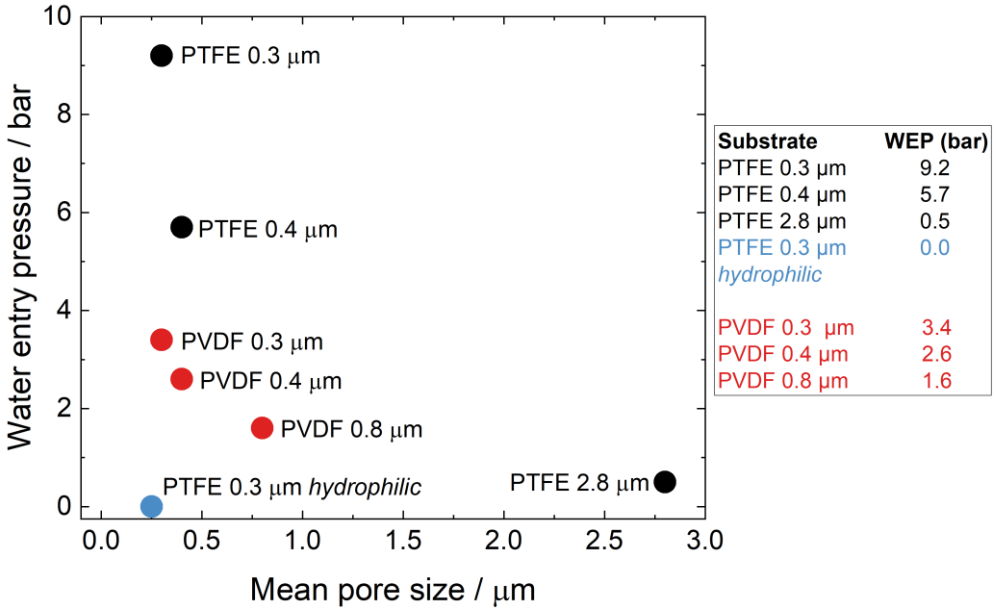

Figure S9. Water entry pressure measured for all substrates used in this work.

10. Chemical analyses of nominally pure Ag samples and Ag/Cu samples

Chemical analyses of the samples were performed with different methods. To compare and assess potential impurity levels at an initial stage, we used X-Ray fluorescence (XRF). Pristine PVDF (0.8 µm pore size) and PTFE (0.4 µm pore size) substrates as well as GDEs based on the same substrates with 500 nm thick Ag layers were analyzed. In the pristine samples, only signals of fluorine and very small impurities of silicon and aluminium (probably from the environment) are visible. The samples after Ag metal deposition naturally show Ag with the a minor sulphur signal, which is very similar in intensity for the PVDF and PTFE-based samples. As sulphur is a common Ag contaminant, minor traces were expected. To more accurately determine the levels of metal impurities most likely to cause selectivity variations, we employed Laser Ablation – Inductively Coupled Plasma Mass Spectroscopy (LA-ICP-MS). By analyzing pristine PTFE and PVDF coated with Ag layers, we looked for the most common metallic contaminants and possible impurities from the sputtering instrument (Li, Na, K, Al, Ca, Fe, Ni, Cu, Pt). As reported in Table 4, no significant difference are visible between the PTFE and PVDF samples, as they have similar concentrations of all contaminants. The concentrations reported were not calibrated for the individual metals in each case, but were normalized to the Ag signal (assumed to be constant) and therefore only provide a relative comparison but not a complete quantitative evaluation.

	Li	Na	Al	K	Ca	Fe	Ni	Cu	Pt
PTFE+Ag pristine									
Signal sum (cts)	245	58514	1382	8220	69	128	2067	341	666
Average signal (norm to Ag)	**0.00006**	**0.0135**	**0.00031**	**0.00163**	**0.00001**	**0.00003**	**0.00048**	**0.00008**	**0.00015**
Standard Deviation	0.00003	0.00392	0.00014	0.00046	0	0.00002	0.00029	0.00001	0.00024
Relative standard deviation %	62.6	29	44.7	28.4	36	71.3	59.5	12.3	155.6
PVDF+Ag pristine									
Signal sum (cts)	434	22252	2934	19179	94	71	3261	334	19
Average signal (norm to Ag)	**0.00009**	**0.00444**	**0.00058**	**0.00366**	**0.00002**	**0.00001**	**0.00063**	**0.00007**	**0**
Standard Deviation	0.00007	0.00126	0.00022	0.00144	0.00001	0.00001	0.00052	0.00001	0
Relative standard deviation %	77.4	28.4	38.5	39.5	71.5	53.6	81.8	20.8	96.1

Table S3. Signal ratio of various potential metal impurities analyzed by LA-ICP-MS for PVDF and PTFE substrates deposited with Ag. The signal ratios are calculated with respect to the Ag quantity, assumed to be constant. The data do not provide a quantitative evaluation, but only a qualitative assessment of the impurity levels.

We also considered the possibility that non-metallic contaminant, invisible to the LA-ICP-MS method, could be responsible for the difference in selectivity. We can expect in particular that O_2 (ubiquitous general contaminant) and S (common Ag contaminant) could potentially play a role. For this, we react a PTFE-based Ag GDE with O_2 (electrochemical oxidation) or with S (exposure to a Na_2S solution). As shown in Fig. S9, however, the application of the reducing potential necessary to reach eCO_2RR conditions leads to the cleaning of the reacted Ag surface and to an electrochemical behavior that is independent of the impurity. This is evidenced by the appearance of reduction peaks in the voltammetry, a single peak for Ag_2O (reduction Ag^+ to Ag) and two peaks for Ag_2S (reduction of bulk Ag_2S first, and then reduction of a residual Ag_2S monolayer), in agreement with literature

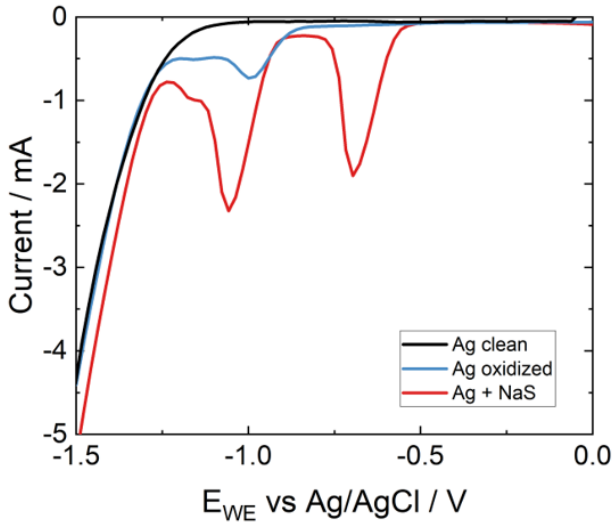

Figure S10. Linear scan voltammetry for a pristine PTFE-based Ag GDE, an electrochemically oxidized (Ag_2O formation) GDE and a GDE that has been exposed to Na_2S and thus reacted with S^{2-} to give Ag_2S.

Since Cu is a metal known to have strong CH4 selectivity, we specifically investigated the composition of nominally pure Ag samples and of Ag samples on which Cu was sputtered for a certain time. To accurately determine the Cu concentration, we calibrated the LA-ICP method using standard samples of Ag (ingots) with different levels of Cu impurities (500 ppm, 100 ppm, 10 ppm) to better reproduce the matrix of our samples. As visible from Table S3, no significant differences are present in the Cu content of PVDF and PTFE samples exposed to Cu sputtering for the same time.

Cu sputtering time (s)	**Ratio of Cu vs Ag (%)** *PVDF samples*	**Ratio of Cu vs Ag (%)** *PTFE samples*
0	0.002	0.002
2	0.035	0.044

10	0.081	0.091
30	0.435	0.403
90	1.12	1.1

Table S4. Cu content analyzed by LA-ICP-MS for PVDF and PTFE substrates deposited with Ag and different amounts of Cu.

11. Long-term experiments: complete product analysis

The complete product distribution of all GDEs involved in the study of long-term stability was assessed including the liquid product formation. As seen in Fig. S10 and S11, only formic acid (HCOOH) could be detected in significant quantities. As the concentration was determined only at the end of the electrolysis, the time dependence of HCOOH formation has been assumed constant over the electrolysis time.

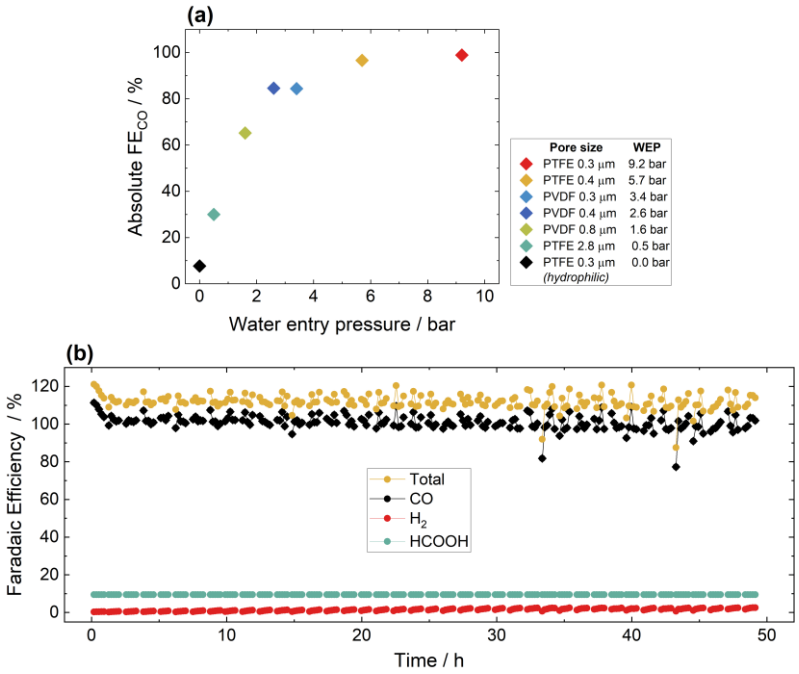

Figure S11. (a) Non-normalized FE_{CO} as a function of water entry pressure. **(b)** Complete, non-normalized product distribution for the long-term stability test performed on a on a 0.3 µm PTFE GDE.

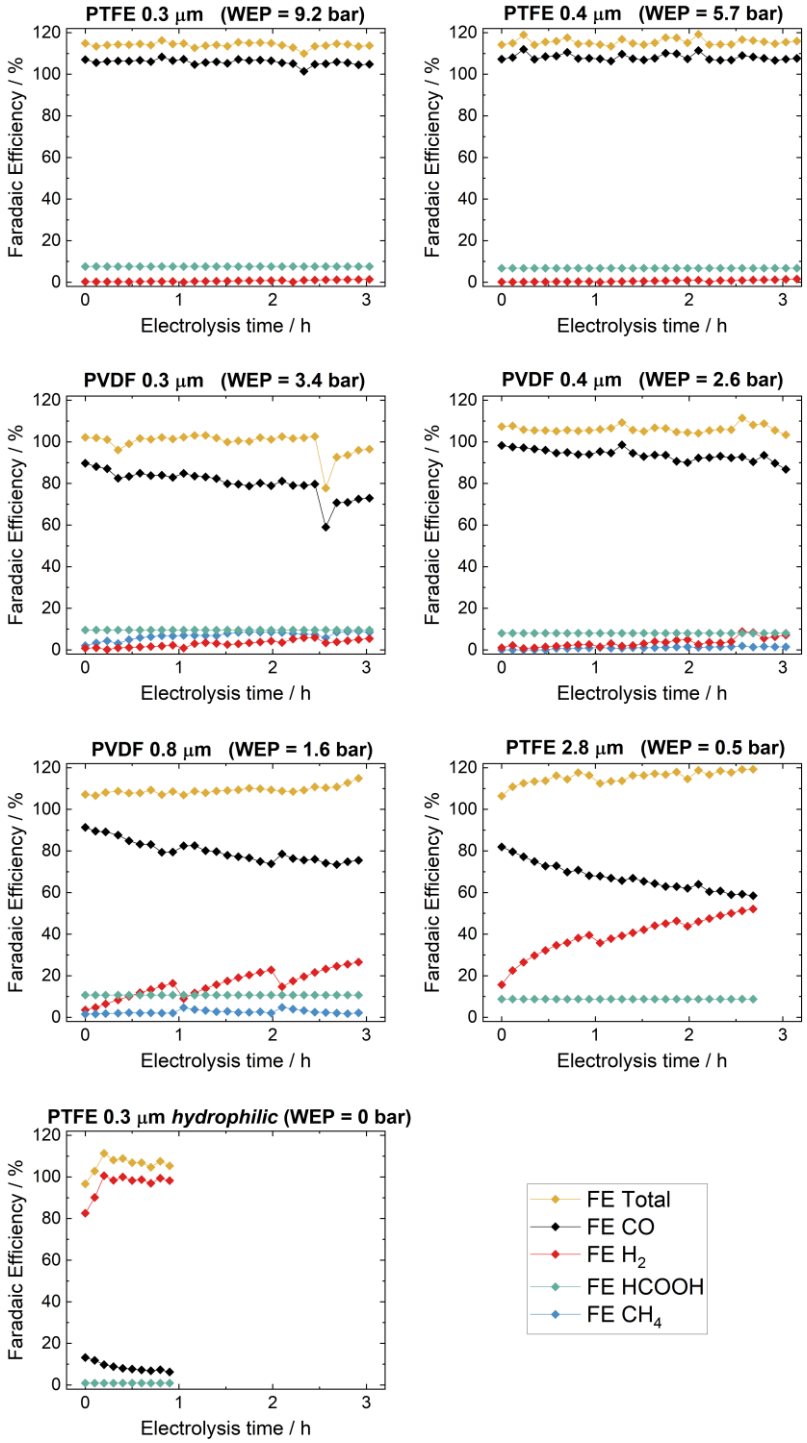

Figure S12. Complete, non-normalized product distribution during the 3-hour stability test, for all the PVDF and PTFE substrates analyzed in this work (noted in the figure). The FE_{CO} data were used to compose Fig. 4b after being normalized to the initial (t=0) values.

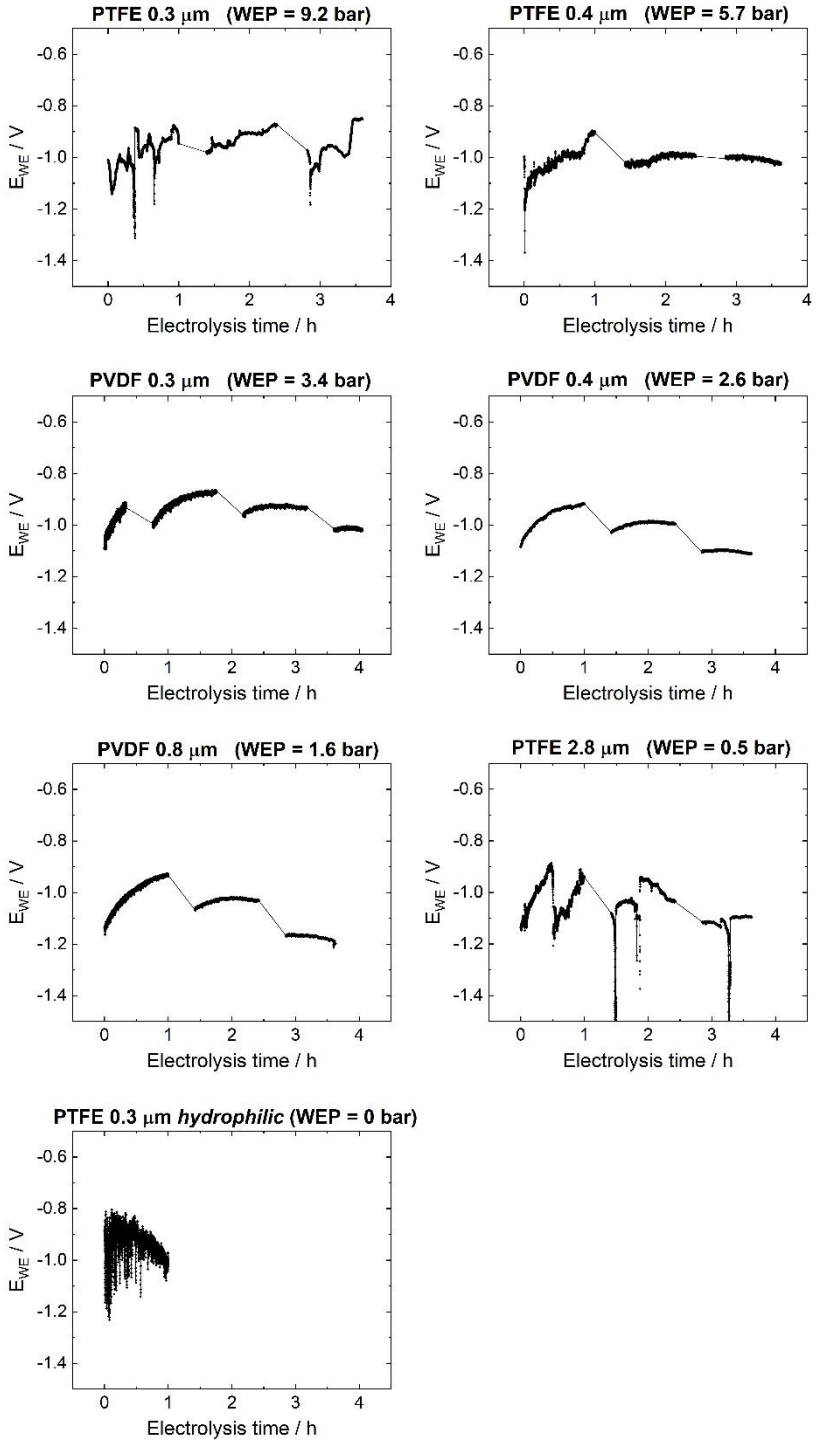

Figure S13. Working electrode voltage as a function of electrolysis time during the 3-h stability test. Thinner GDEs show a much noisier signal due to bubble formation. In all cases, the voltage does not show a linear trend. In addition, inspection of the initial and final values do not show a clear shift of the voltage, but rather an initial activation to less negative potentials, followed by a decay. We note that, even during the activation period, the selectivity is still decaying towards a more pronounced H_2 evolution.

12. Ag samples with Cu addition: complete product analysis

When analyzing samples with up to 1% of Cu added to a pristine Ag layer, a more complex product distribution is observed (Fig. S14). Besides CO, CH_4, C_2H_4 and HCOOH were found as main components, and several minor products such as acetaldehyde, propionaldehyde, ethanol and 1-propanol were also observed in the GC chromatogram (all below 5 ppm, i.e. FE << 1 %). Ethanol and 1-propanol were also identified by NMR (concentrations of ca. 0.1 mM, FE << 1 %). Curiously, all the GDEs require similarly negative voltages to achieve 100 mA/cm^2 of current, comparable with pure Ag catalysts, and show no shift to less negative voltages with Cu insertion, possibly indicating a synergistic effect of Ag and Cu in the CO_2RR.

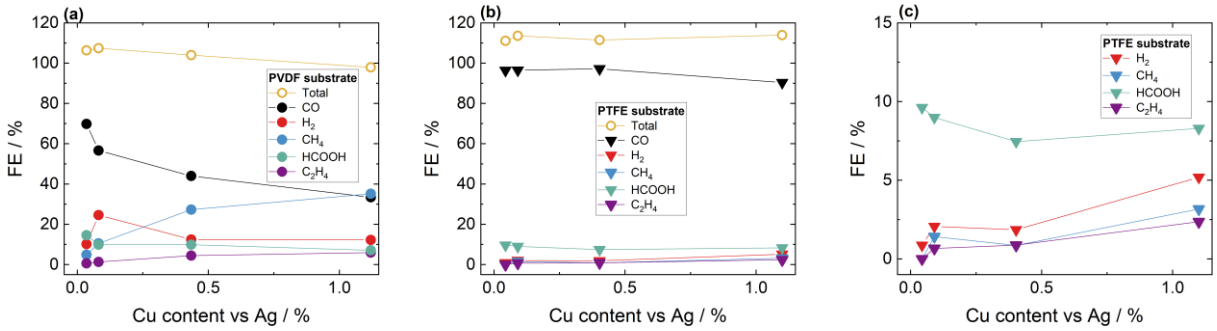

Figure S14. Product formation as a function of Cu content for GDEs prepared on PVDF and PTFE substrates by sputtering a pristine layer of Ag, and subsequently a defined amount of Cu on top. Product distribution obtained on **(a)** PVDF substrates and **(b)** PTFE substrates (magnification of the range of FE< 15 % shown in **(c)**).

13. Reference

1. Ju, W. *et al.* Sn-decorated Cu for selective electrochemical CO2 to CO conversion: Precision architecture beyond composition design. *ACS Appl. Energy Mater.* **2**, 867–872 (2019).
2. Ju, W. *et al.* Electrocatalytic Reduction of Gaseous CO2 to CO on Sn/Cu-Nanofiber-Based Gas Diffusion Electrodes. *Adv. Energy Mater.* **9**, 1901514 (2019).
3. Moret, S., Dyson, P. J. & Laurenczy, G. Direct, in situ determination of pH and solute concentrations in formic acid dehydrogenation and CO2 hydrogenation in pressurised aqueous solutions using 1H and 13C NMR spectroscopy. *Dalt. Trans.* **42**, 4353–4356 (2013).
4. Birss, V. I. & Wright, G. A. The kinetics of the anodic formation and reduction of phase silver sulfide films on silver in aqueous sulfide solutions. *Electrochim. Acta* **26**, 1809–1817 (1981).